Amorphous mesoporous calcium carbonate and magnesium carbonate as effective sorbents for the removal of phosphate in aqueous solutions

Eveline Croket, Michelle Åhlén, Maria Strømme and Ocean Cheung*

Division of Nanotechnology and Functional Materials, Department of Materials Science and Engineering, Uppsala University, Ångström Laboratory, Uppsala SE-751 03, Box 35, Sweden.

*Corresponding author. Tel.: +46 18 471 3279, E-mail: ocean.cheung@angstrom.uu.se

Abstract

In this work, highly porous amorphous calcium carbonate (HPACC) and mesoporous magnesium carbonate (MMC) were tested as potential phosphate (PO_4^{3-}) sorbents in water. The performance of these sorbents at a PO_4^{3-} initial concentration between 0 – 1000 mg/L was evaluated. These highly porous materials were found to have enhanced PO_4^{3-} uptake at low concentrations (<100 mg/L) when compared with commercial $CaCO_3$ and $MgCO_3$. The enhanced uptake on HPACC and MMC at low concentration was due to the high surface area and the porosity of these sorbents. The presence of NaCl salt of up to 1000 mg/L had very little effect on the performance of HPACC (<10% decreased uptake capacity), but the PO_4^{3-} uptake on MMC reduced to close to zero. HPACC with its high PO_4^{3-} uptake at low concentration could be relevant for real life application of PO_4^{3-} ions removal from water.

Keywords: Phosphate, Adsorption, Calcium carbonate, Magnesium carbonate

Introduction

Eutrophication of surface and freshwater sources remains a serious issue in today's society with wide reaching economic and environmental consequences. The weathering and erosion of bedrock represent natural processes that affect the phosphorus levels in many lakes [1]. However, it is undeniable that anthropogenic sources, such as agricultural run-off, municipal wastewater and industrial effluence, greatly contribute to the eutrophication of aquatic systems. The anthropogenic enrichment of phosphorus in such bodies of water not only contribute to the deterioration of the water quality but also lead to oxygen depletion due to the excessive growth of aquatic plants and microalgae. Resulting in detrimental effects on the marine ecosystem [2, 3]. As such, several methods have been developed for the removal of phosphate in aqueous systems, which can be divided into three principal classes, namely, biological and chemical processes and physical filtration. The use of biological processes mainly involves the removal of phosphate through plants and microorganisms, e.g. halophytes, polyphosphate accumulating organisms and microalgae. On the other hand, chemical processes rely on phosphate removal through precipitation and flocculation using metal salts and polymers. Finally, physical filtration typically utilizes membranes and sand. Some of these methods have been used with great success to treat elevated phosphate levels in water, e.g. the use of metal salts in wastewater treatment plants [4, 5]. However, despite their widespread use, many of these methods suffer from a number of drawbacks that limit their efficiency. These drawbacks include the production of heavy metal sludge and polluting by-products, narrow working conditions, limited removal efficiency, and high cost etc. [3, 6]. Adsorption processes offers an appealing alternative solution to some of these problems due to their high efficiency, low cost, minimal formation of polluting by-products, sorbent reusability and phosphate recoverability [6]. Phosphate

concentration below that of 0.1 mg/L may also be reached by using sorbents with high adsorption capacities[3]. Which could decrease phosphate-induced algal and cyanobacterial blooms and in turn prevent accelerated eutrophication. Various sorbents have been investigated in regards to phosphate adsorption in aqueous systems, ranging from biochars and activated carbons [7-9], metal-organic frameworks [10-12], metal oxides and hydroxides [13-18], to name a few. The application of calcium and magnesium carbonate-based sorbents for phosphate removal have however remained relatively unexplored despite their widespread abundance in nature. Studies have shown that phosphate ions are able to effectively interact with both Ca^{2+}-ions and Mg^{2+}-ions. In the case of calcite the interactions may results in either precipitation, forming calcium phosphate species, or adsorption which primarily takes place at concentrations below 0.2 μmol PO_4^{3-}/g [19, 20]. The uptake capacity of has been found to be limited by the number of specific adsorption sites on the accessible surface of the material. As the sites become occupied by adsorbed phosphate ions, lateral interactions between the adsorbed species and free ions occur, leading to the formation of clusters that may act as nucleation sites for the growth of calcium phosphate [20]. As such, factors restricting the use of calcite as an efficient sorbent for phosphate removal may be due to its limited adsorption capacity, particularly at high phosphate concentrations. The use of amorphous calcium and magnesium carbonates may offer an advantage compared to their crystalline counterparts in this regard due to their high surface areas. In recent years, our group has developed a number of highly porous inorganic materials with very high specific surface area. These materials include mesoporous magnesium carbonate (MMC) [21, 22] and highly porous amorphous calcium carbonate (HPACC) [23]. MMC and HPACC share a similar microstructure. They are constructed with nanometer-sized

particles that have aggregated together, forming a bulk particle with highly a porous structure. The high specific surface area and porosity allow these materials to have excellent sorption properties. Furthermore, the pore surface can be functionalized to tailor the chemistry of these materials. We have investigated and optimized these materials for a number of different applications including gas separation [24], drug delivery [23, 25-29], and adsorption of organic pollutants such as Azo dyes from water [30]. In this study, we will explore the utilization of MMC and HPACC as sorbents for the removal of phosphate from water. The high porosity of these materials, in conjunction with high affinity between calcium/magnesium ions and phosphate ions, could render them promising phosphate sorbents with high sorption kinetics.

2. Experimental section

2.1 Materials

Methanol (MeOH), Nitric acid (HNO_3, 65 %) and Calcium oxide (CaO) were purchased from VWR International AB, Sweden and Monopotassium phosphate (H_2KPO_4) and Magnesium oxide (MgO) were purchased from Sigma-Aldrich, USA.

All chemicals were used as received without further purification.

2.2 Synthesis of highly porous amorphous calcium carbonate (HPACC)

HPACC was prepared according to procedures previously published by our group [23]. In summary, 75 ml MeOH was placed into a glass reaction vessel (350 ml, Andrew glass co.) and heated in an oil batch at 50 ˚C while stirring under 4 bar of CO_2 pressure. Thereafter, 1.25 g of CaO was added to the warm MeOH and the reaction mixture was left stirring under the previously mentioned conditions for 4 hours. The obtained milky dispersion was thereafter centrifuged at 3,800 rpm for 15 minutes in order to remove

unreacted CaO particles, and a colloidal HPACC suspension was obtained. The HPACC suspension was then finally dried at 150 ˚C for 4 – 5 hours in a ventilated.

2.3 Synthesis of amorphous mesoporous magnesium carbonate (MMC)

MMC was synthesized according to procedures previously published by our group [21]. Briefly, 10 g of MgO was dispersed in 150 ml MeOH and the reaction mixture was left stirring in a glass reaction vessel (350 ml, Andrew glass co.) pressurized at 4 bar CO_2 for 24 h. The obtained cloudy mixture was centrifuged at 3,800 rpm for 30 minutes producing a yellow tinged colloidal MMC suspension. A pre-dried gel was then produced by heating the MMC suspension in a warm water bath under constant manual stirring, after which the gel was finally dried at 150 ˚C for 24 hours in a ventilated oven.

2.4 Surface area and porosity measurements

The specific surface area and porosity of the samples were determined by nitrogen sorption at 77 K using a Micromeritics ASAP 2020 Surface Area and Porosity Analyzer (Norcross, GA, USA). Samples were pre-treated at 373 K for 6 hours under dynamic vacuum (1×10^{-4} Pa) using a Micromeritics Smart VacPrep sample preparation unit (Norcross, GA, USA) prior to analysis.

2.5 Powder X-ray diffraction

Powder X-ray diffraction (PXRD) analysis was performed on a Bruker D8 Advanced TWIN/TWIN powder diffractometer (Billerica, WIS, USA) operated at 40 kV and 40 mA, using Cu kα radiation (λ = 1.5418 Å), step-size 0.04˚ and a measuring time of 2 seconds per step.

2.6 Scanning electron microscopy

The morphology of the samples were studied using a Zeiss LEO 1530 scanning electron microscope (SEM) (Oberkochen, Germany) operated at kV. Samples were prior to imaging sputter-coated with a layer of Ag/Pd.

2.7 Inductive coupled plasma optical emission spectroscopy

Inductive coupled plasma optical emission spectroscopy (ICP-OES) analysis was carried out on a PerkinElmer Avio 200 ICP Optical Emission Spectrometer (Waltham, MA, USA) using normal argon gas flow and axial plasma. All standard and sample solutions were acidified to 2 v/v % using 65 % HNO_3 and filtered (0.45µm cellulose acetate membrane filters, VWR International AB, Sweden) prior to analysis. Blank solutions were acidified to 5 – 10 v/v % using 65 % HNO_3. Each analysis was carried out in triplicates and the measurements were done by element. Na- and P-standards were purchased from PerkinElmer.

2.8 Phosphate adsorption study

Phosphate adsorption studies were carried out on HPACC, MMC, commercial $CaCO_3$ and commercial $MgCO_3$ at room temperature. Each sorbent (1 mg/mL) was dispersed in a 15 ml or 50 ml Falcon tube containing phosphate solutions of concentrations between 0 – 1000 mg/ml. The dispersions were then left shaking on a Heidolph Multi Reax orbital shaker (Schwabach, Germany) at 1,000 rpm for 24 hours, after which the they were filtered (0.45µm cellulose acetate membrane filters, VWR International AB, Sweden) and the phosphate concentration determined using ICP-OES.

The phosphate standard solution used in the study was prepared by dissolving approximately 1.43 g of KH_2PO_4 in 1000 ml ultra-pure water, resulting in final phosphate concentration of 1000 mg/ml. Phosphate solutions for the adsorption study

were prepared by diluting the standard solution by addition of ultra-pure water until the desired concentrations were obtained. The exact PO_4^{3-} concentration of each solution before adsorption experiments were determined by ICP-OES in order to obtain the correct PO_4^{3-} initial concentration of each individual experiments and to minimize the errors, as we had found that there was a large variation of PO_4^{3-} initial concentrations even between standard solutions prepared in the same way.

3. Results and discussion

3.1 Sorbent characterization

The synthesized HPACC and MMC were characterized in order to ensure the quality of the sorbents. The PXRD diffractograms displayed in Figure 1a show that HPACC and MMC were both X-ray amorphous and SEM images (Figure 2) show that the materials were constructed from aggregated spherical nanoparticles. The nitrogen sorption isotherms of HPACC and MMC (Figure 1b) both exhibit a reversible type IV shape indicative of mesoporous adsorbents according to IUPAC classifications [31]. The sorbents were found to be porous with a specific Brunauer–Emmett–Teller (BET) surface area of 343 and 561 m^2/g for HPACC and MMC, respectively. These observations are in good agreement with our previous findings, and for further discussions regarding the characterization of these materials, we refer the readers to our previous publications [21, 23].

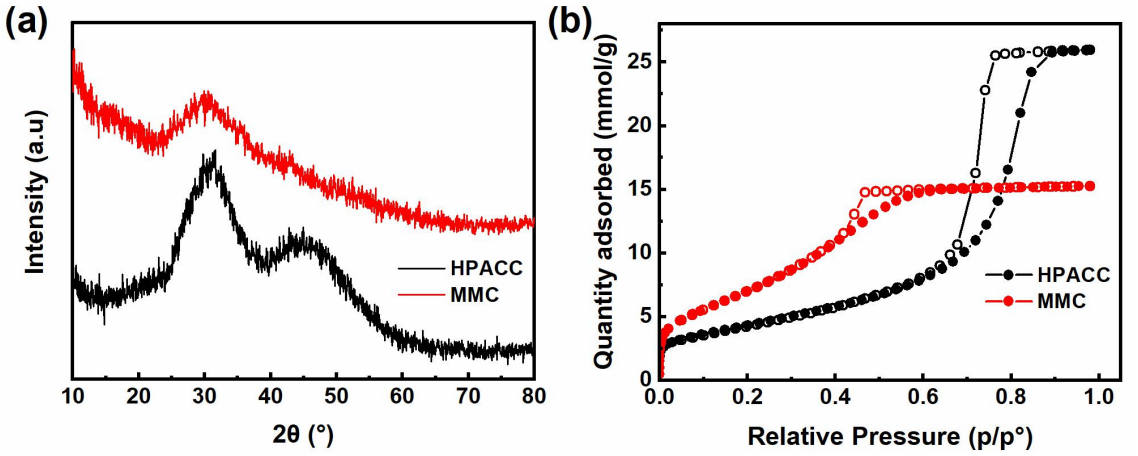

Figure 1. (a) PXRD diffractograms and (b) nitrogen sorption isotherms of HPACC and MMC.

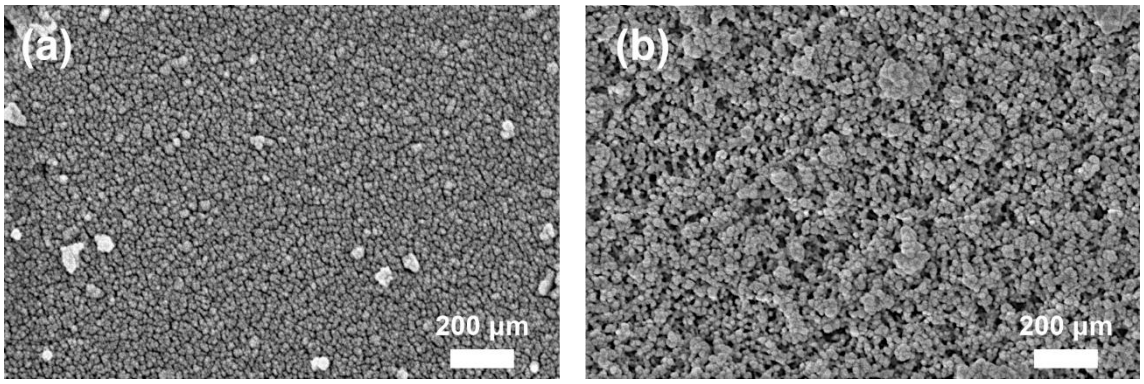

Figure 2. SEM images of (a) MMC and (b) HPACC.

3.2 Phosphate adsorption on HPACC and MMC

The phosphate uptake on HPACC, MMC, commercial $CaCO_3$ and commercial $MgCO_3$ at 24 h at initial concentrations of 10 – 1000 mg PO_4^{-3}/ml are shown in Figure 3a-d. All tested sorbents displayed noticeable phosphate uptake. The trend in phosphate adsorption was found to be comparable for all materials, wherein the uptake of PO_4^{3-} increased with increasing PO_4^{3-} concentration.

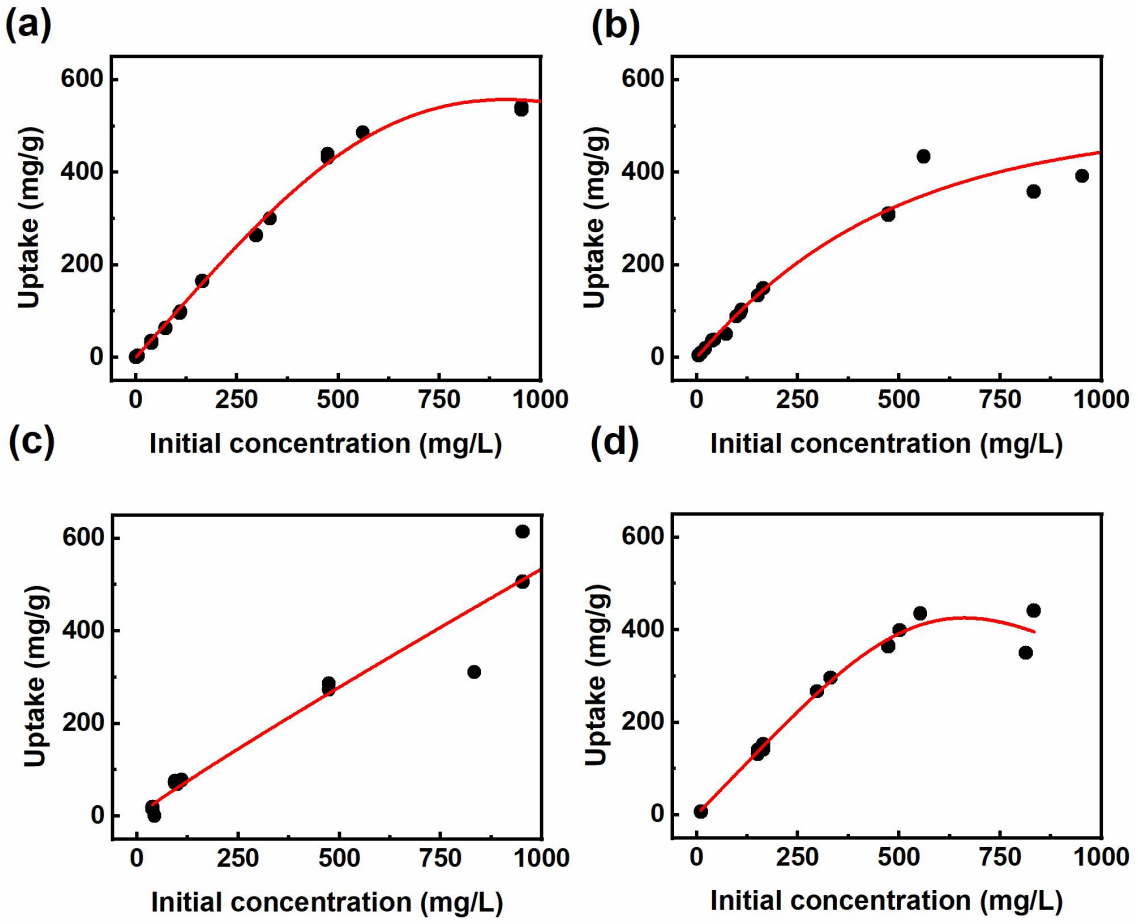

Figure 3. PO_4^{3-} uptake on a) HPACC, b) MMC, c) commercial $CaCO_3$ and d) commercial $MgCO_3$ varying initial PO_4^{3-} concentrations. The variation in the initial concentrations for the different samples were due to the difference between the expected and real concentrations in the standard solutions before the adsorption experiments, as discussed in the experimental section.

The equilibrium adsorption isotherms (Figure 4a-d) show comparable PO_4^{3-} uptakes for both the synthesized sorbents and their commercial counterparts at relatively high concentrations, more specifically above 300 mg PO_4^{-3}/L and 50 mg PO_4^{-3}/L for the $CaCO_3$-based and $MgCO_3$-based sorbents, respectively. An enhanced PO_4^{-3} adsorption was however observed on HPACC and MCC below these concentrations compared to commercial $CaCO_3$ and $MgCO_3$. This observation could most likely be attributed to the

increased surface area of the HPACC and MMC sorbents when compared with $CaCO_3$ and $MgCO_3$. The high surface area HPACC and MMC sorbents had and increased number of high-energy sorption sites within the pores of these sorbents. These high-energy sites would in turn lead to an enhanced the surface interaction between the sorbents and PO_4^{-3} ions, particularly at low concentrations. Table 1 shows a comparison between HPACC, MMC and other sorbents. Table 1 compares the PO_4^{3-} uptake of the synthesized sorbents with those available in the literature. Unfortunately, given the difference in the initial concentrations used in the different study, it is difficult to make direct comparisons between the different sorbents. On the other hand, the sorbents presented in this study showed a reasonable level of PO_4^{3-} uptake both at low initial concentration and at high initial concentrations.

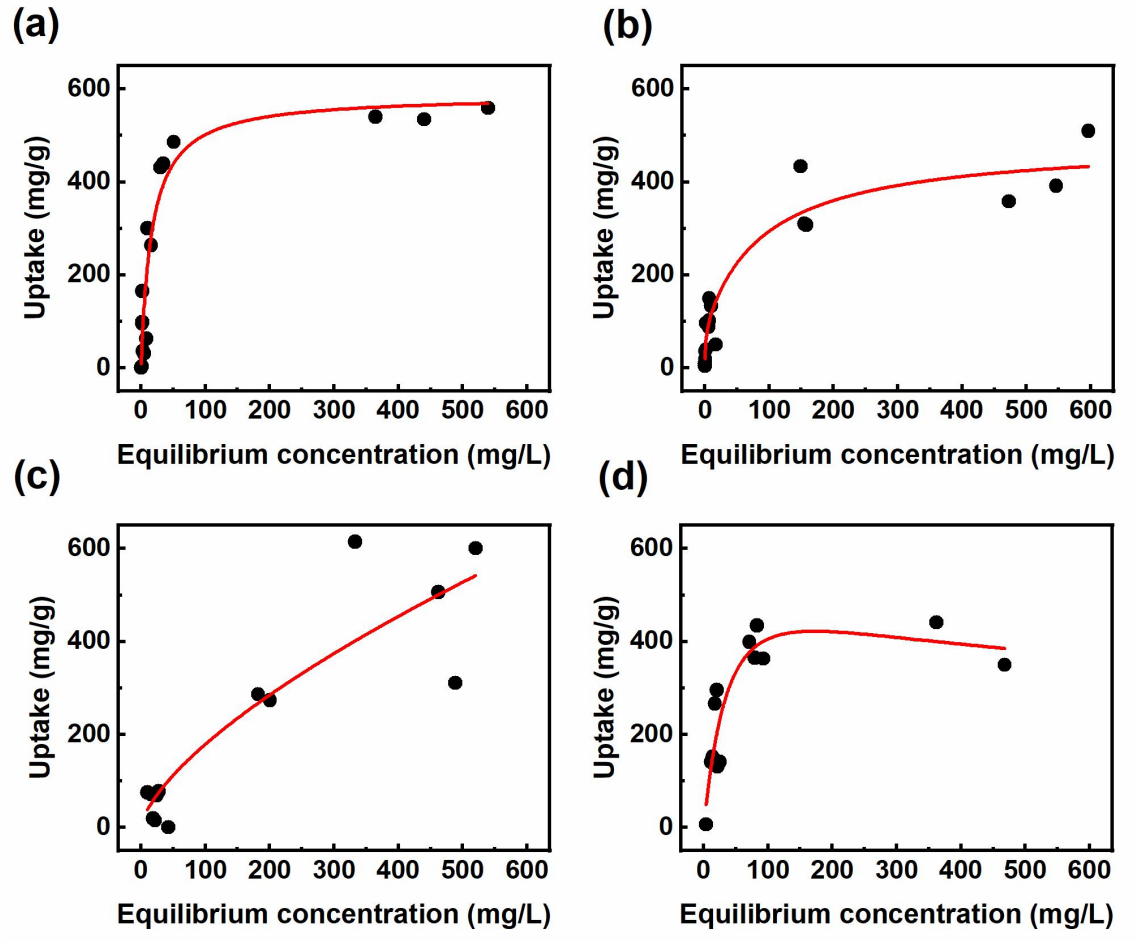

Figure 4. Equilibrium PO_4^{3-} uptake of a) HPACC, b) MMC, c) commercial $CaCO_3$, and d) commercial $MgCO_3$.

Table 1. Comparison between the phosphate uptake on the sorbents explored in the study and other materials.

Materials	**Initial PO_4^{3-} concentration (mg/L)**	**Sorbent dosage (g/L)**	**PO_4^{3-} uptake (mg/g)**	**Reference**
HPACC	953	1.1	540	This study
	38	1.0	36	
MMC	953	1.0	391	
	38	1.0	36	
Commercial $CaCO_3$	953	1.0	506	
	38	1.1	15	

Commercial $MgCO_3$	833 38	1.0 1.0	440 7	
CP-Fe-I CTAB CTAB-IONP nZVI Steel slag	50 10 10 90 11	2 2 2 0.4 40	22.1 1.2 4.9 116 0.2	[1]
Fe-IRMOF-3-10	500	1	179	[32]
MIL-100-(Fe)	8	0.07	93.5	[33]
La@ZIF-8* ZIF-8*	70 70	- -	147.6 61.4	[34]
Iron-impregnated WAS biochar*	1000	2	82.5	[35]
Fe-Mn binary oxide (Fe/Mn = 6:1)	10	0.2	26	[36]
1Fe-HNT	10	3	2.1	[37]
Lanthanum carbonate nanorods*	100	0.2	303	[38]
$La(OH)_3/Fe_3O_4$ (4:1)*	15	0.1	74	[18]
LAH-1/10	80	1	68	[39]
Phoslock®*	10	1	10.6	[40]
Dolomite	100	2	48	[41]
am-ZrO_2	10	0.1	64	[15]
Ti-OMS (20:1) Fe-OMS (20:1) Zr-OMS (20:1) Al-OMS (20:1)	1 1 1 1	10 10 10 10	4.4 4.3 4.4 3.2	[42]
Mg-ACC * (Mg/Ca = 4:6)	1425	5	198	[43]

3.3 Phosphate adsorption kinetics

We further tested the PO_4^{3-} uptake kinetics (with an initial PO_4^{3-} concentration of 100 mg/L) on these sorbents and the results are shown in Figure 5. Activated carbon was also added to this test for comparison. It is clear from Figure 5 that the increased

porosity on MMC and HPACC had a significant effect on the sorption rate and amount of PO_4^{3-} at this initial concentration level of 100 mg/L. HPACC showed the fastest relative uptake of PO_4^{3-} when compared with all the other tested sorbents. Over 80 mg/g of PO_4^{3-} uptake was recorded on HPACC within 2 hours, whereas all the other tested sorbents took up less than 10 mg/g within the same time. Although significantly lower than HPACC, MMC showed higher uptake than commercial $MgCO_3$, $CaCO_3$ and activated carbon after 2 hours. After 16 hours the uptake of PO_4^{3-} on HPACC was around 100 mg/g, around 60 mg/g for MMC and around 40 mg/g for commercial $CaCO_3$. The data presented here clearly shows that at low initial concentration (i.e. 100 mg/L), HPACC has significant advantages over the other tested sorbents both in terms of the uptake capacity and the uptake rate. This enhancement is likely to be the effect of the increased specific surface area and porosity.

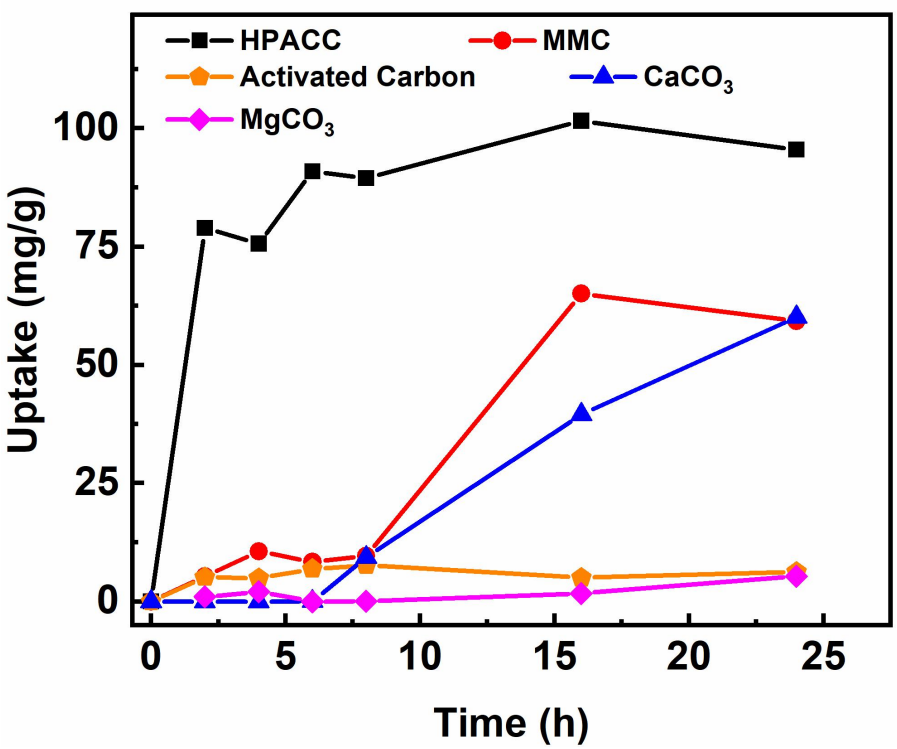

Figure 5. Phosphate adsorption kinetics of different sorbents. The initial PO_4^{3-} concentration was set at 100 mg/L.

3.4 The effect of salt

The effect of salt on the uptake of PO_4^{3-} on HPACC and MMC was tested by conducting the PO_4^{3-} sorption experiments on a 500 mg/L PO_4^{3-} solution with NaCl concentration of up to 1000 mg/L. Figure 6 shows that the uptake of PO_4^{3-} on HPACC was not significantly affected by the presence of NaCl, a slight decrease in the uptake of around 10% was noted when the NaCl concentration was over 50 mg/L. In contrast, the PO_4^{3-} uptake on MMC was noticeably affected by the presence of NaCl. The uptake of PO_4^{3-} on MMC decreased with increasing NaCl concentration and when the NaCl concentration reached 1000 mg/L, the PO_4^{3-} uptake was reduced to close to zero. These observations suggested that the Cl^- ions binds much more strongly to Mg than to Ca, as a result, the effect of NaCl on the PO_4^{3-} uptake on HPACC was not as significant.

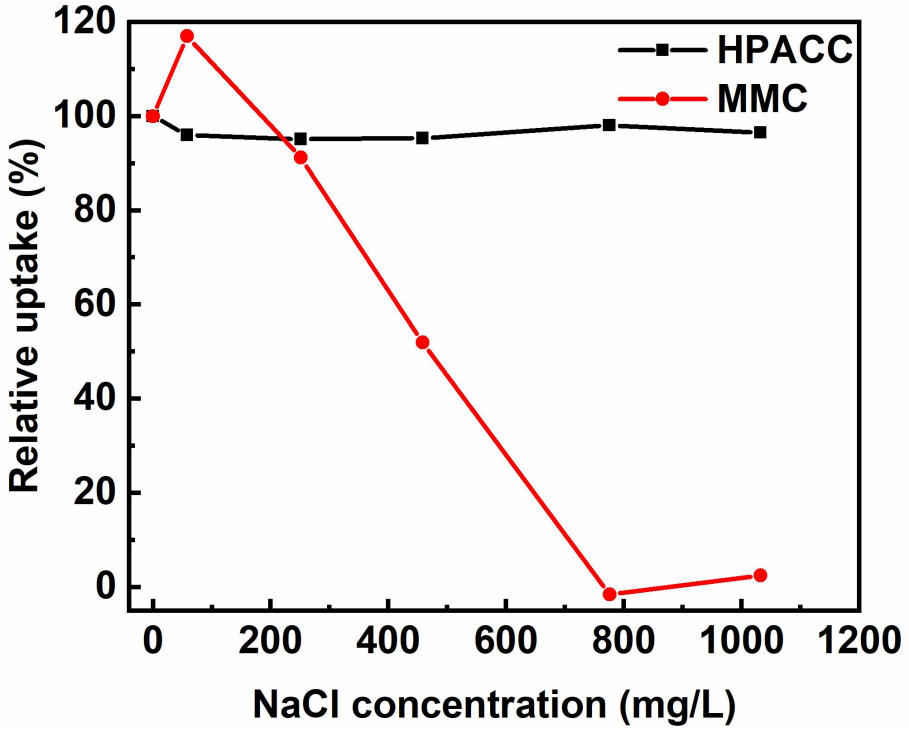

Figure 6. Phosphate adsorption kinetics of HPACC and MMC in the presence of NaCl salt, initial PO_4^{3-} concentration was set at 500 mg/L.

4. Conclusion

In this work, we tested the PO_4^{3-} ion sorption properties of a number of highly porous carbonate-based sorbents. Highly porous amorphous calcium carbonate, HPACC, showed very high uptake of PO_4^{3-} ions at low concentrations (< 100 mg/L). The increased porosity and surface area over the commercial $CaCO_3$ was responsible for the increased uptake at low PO_4^{3-} concentration. Mesoporous magnesium carbonate, MMC, also showed enhanced PO_4^{3-} uptake at low concentration over the commercial $MgCO_3$. The presence of NaCl at up to 1000 mg/g had insignificant effects on the performance of HPACC, 90% of the PO_4^{3-} uptake was observed even at a NaCl concentration of 1000 mg/L. On the other hand, the PO_4^{3-} uptake capacity on MMC diminished when the NaCl concentration increased. HPACC could be further developed into an effective

PO_4^{3-} ion sorbent given its high porosity and specific surface area, which has shown enhanced PO_4^{3-} uptake over other sorbents, particularly at low PO_4^{3-} concentrations.

Acknowledgements

The authors thank the Swedish Research Council for Sustainable Development (FORMAS, Grant No. 2018-00651) and Åforsk Foundation (Grant No. 19-549) for their financial support.

References

[1] Mahmoud, A. S., Mostafa, M. K., Nasr, M. Regression model, artificial intelligence, and cost estimation for phosphate adsorption using encapsulated nanoscale zero-valent iron. *Sep Sci Technol*. **2018**, 54(1):13-26. https://doi.org/10.1080/01496395.2018.1504799

[2] Menesguen, A., Desmit, X., Duliere, V., Lacroix, G., Thouvenin, B., Thieu, V., Dussauze, M. How to avoid eutrophication in coastal seas? A new approach to derive river-specific combined nitrate and phosphate maximum concentrations. *Sci Total Environ*. **2018**, 628-629:400-14. https://doi.org/10.1016/j.scitotenv.2018.02.025

[3] Kumar, P. S., Korving, L., van Loosdrecht, M. C. M., Witkamp, G. J. Adsorption as a technology to achieve ultra-low concentrations of phosphate: research gaps and economic analysis. *Water Res*. **2019**, 4:100029. https://doi.org/10.1016/j.wroa.2019.100029

[4] Yeoman, S., Stephenson, T., Lester, J. N., Perry, R. The removal of phosphorus during wastewater treatment: a review. *Environ Pollut*. **1988**, 49(3):183-233. https://doi.org/10.1016/0269-7491(88)90209-6

[5] Ye, Y., Ngo, H. H., Guo, W., Liu, Y., Li, J., Liu, Y., Zhang, X., Jia, H. Insight into chemical phosphate recovery from municipal wastewater. *Sci Total Environ*. **2017**, 576:159-71. https://doi.org/j.scitotenv.2016.10.078

[6] De Gisi, S., Lofrano, G., Grassi, M., Notarnicola, M. Characteristics and adsorption capacities of low-cost sorbents for wastewater treatment: A review. *SM&T*. **2016**, 9:10-40. https://doi.org/10.1016/j.susmat.2016.06.002

[7] Huang, Y., Lee, X., Grattieri, M., Yuan, M., Cai, R., Macazo, F. C., Minteer, S. D. Modified biochar for phosphate adsorption in environmentally relevant conditions. *Chem Eng Technol*. **2020**, 380. https://doi.org/10.1016/j.cej.2019.122375

[8] Han, T., Lu, X., Sun, Y., Jiang, J., Yang, W., Jonsson, P. G. Magnetic bio-activated carbon production from lignin via a streamlined process and its use in phosphate removal from aqueous solutions. *Sci Total Environ*. **2020**, 708:135069. https://doi.org/10.1016/j.scitotenv.2019.135069

[9] Yin, Q., Ren, H., Wang, R., Zhao, Z. Evaluation of nitrate and phosphate adsorption on Al-modified biochar: Influence of Al content. *Sci Total Environ*. **2018**, 631-632:895-903. https://doi.org/10.1016/j.scitotenv.2018.03.091

[10] Luo, F., Feng, X., Li, Y., Zheng, G., Zhou, A., Xie, P., Wang, Z., Tao, T., Long, X., Wan, J. Magnetic amino-functionalized lanthanum metal-organic framework for selective phosphate removal from water. *Colloids Surf A Physicochem Eng Asp*. **2020**, 611. https://doi.org/10.1016/j.colsurfa.2020.125906

[11] Hassan, M. H., Stanton, R., Secora, J., Trivedi, D. J., Andreescu, S. Ultrafast removal of phosphate from eutrophic waters using a cerium-based metal-organic framework. *ACS Appl Mater Interfaces*. **2020**, 12(47):52788-96. https://doi.org/10.1021/acsami.0c16477

[12] Lin, K.-Y. A., Chen, S.-Y., Jochems, A. P. Zirconium-based metal organic frameworks: highly selective adsorbents for removal of phosphate from water and urine. *Mater Chem Phys*. **2015**, 160:168-76. https://doi.org/10.1016/j.matchemphys.2015.04.021

[13] Ajmal, Z., Muhmood, A., Usman, M., Kizito, S., Lu, J., Dong, R., Wu, S. Phosphate removal from aqueous solution using iron oxides: Adsorption, desorption and regeneration characteristics. *J Colloid Interface Sci*. **2018**, 528:145-55. https://doi.org/10.1016/j.jcis.2018.05.084

[14] Xie, J., Lin, Y., Li, C., Wu, D., Kong, H. Removal and recovery of phosphate from water by activated aluminum oxide and lanthanum oxide. *Powder Technol*. **2015**, 269:351-7. https://doi.org/10.1016/j.powtec.2014.09.024

[15] Su, Y., Cui, H., Li, Q., Gao, S., Shang, J. K. Strong adsorption of phosphate by amorphous zirconium oxide nanoparticles. *Water Res*. **2013**, 47(14):5018-26. https://doi.org/10.1016/j.watres.2013.05.044

[16] Chitrakar, R., Tezuka, S., Sonoda, A., Sakane, K., Ooi, K., Hirotsu, T. Selective adsorption of phosphate from seawater and wastewater by amorphous zirconium hydroxide. *J Colloid Interface Sci*. **2006**, 297(2):426-33. https://doi.org/10.1016/j.jcis.2005.11.011

[17] Gypser, S., Hirsch, F., Schleicher, A. M., Freese, D. Impact of crystalline and amorphous iron- and aluminum hydroxides on mechanisms of phosphate adsorption and desorption. *J Environ Sci*. **2018**, 70:175-89. https://doi.org/10.1016/j.jes.2017.12.001

[18] Wu, B., Fang, L., Fortner, J. D., Guan, X., Lo, I. M. C. Highly efficient and selective phosphate removal from wastewater by magnetically recoverable La(OH)3/Fe3O4 nanocomposites. *Water Res*. **2017**, 126:179-88. https://doi.org/10.1016/j.watres.2017.09.034

[19] Martin, E., Lalley, J., Wang, W., Nadagouda, M. N., Sahle-Demessie, E., Chae, S. R. Phosphate recovery from water using cellulose enhanced magnesium carbonate pellets: Kinetics, isotherms, and desorption. *Chem Eng J*. **2018**, 352:612-24. https://doi.org/10.1016/j.cej.2018.06.183

[20] Liu, Y., Sheng, X., Dong, Y., Ma, Y. Removal of high-concentration phosphate by calcite: effect of sulfate and pH. *Desalination*. **2012**, 289:66-71. https://doi.org/10.1016/j.desal.2012.01.011

[21] Cheung, O., Zhang, P., Frykstrand, S., Zheng, H., Yang, T., Sommariva, M., Zou, X., Strømme, M. Nanostructure and pore size control of template-free synthesised mesoporous magnesium carbonate. *RSC Adv*. **2016**, 6(78):74241-9. https://doi.org/10.1039/c6ra14171d

[22] Frykstrand, S., Forsgren, J., Mihranyan, A., Strømme, M. On the pore forming mechanism of Upsalite, a micro- and mesoporous magnesium carbonate. *Microporous Mesoporous Mater*. **2014**, 190:99-104. https://doi.org/10.1016/j.micromeso.2013.12.011

[23] Sun, R., Zhang, P., Bajnóczi, É. G., Neagu, A., Tai, C.-W., Persson, I., Strømme, M., Cheung, O. Amorphous calcium carbonate constructed from nanoparticle aggregates with unprecedented surface area and mesoporosity. *ACS Appl Mater Interfaces*. **2018**, 10(25):21556-64. https://doi.org/10.1021/acsami.8b03939

[24] Vall, M., Hultberg, J., Strømme, M., Cheung, O. Carbon dioxide adsorption on mesoporous magnesium carbonate. *Energy Procedia*. **2019**, 158:4671-6. https://doi.org/10.1016/j.egypro.2019.01.738

[25] Zhang, P., Zardán Gómez de la Torre, T., Forsgren, J., Bergström, C. A. S., Strømme, M. Diffusion-controlled drug release from the mesoporous magnesium carbonate Upsalite. *J Pharm Sci*. **2016**, 105(2):657-63. https://doi.org/10.1002/jps.24553

[26] Zhang, P., Forsgren, J., Strømme, M. Stabilisation of amorphous ibuprofen in Upsalite, a mesoporous magnesium carbonate, as an approach to increasing the aqueous solubility of poorly soluble drugs. *Int J Pharm*. **2014**, 472(1-2):185-91. https://doi.org/10.1016/j.ijpharm.2014.06.025

[27] Zhang, P., Zardán Gómez de la Torre, T., Welch, K., Bergström, C. A. S., Strømme, M. Supersaturation of poorly soluble drugs induced by mesoporous magnesium carbonate. *Eur J Pharm Sci*. **2016**, 93:468-74. https://doi.org/10.1016/j.ejps.2016.08.059

[28] Vall, M., Zhang, P., Gao, A., Frykstrand, S., Cheung, O., Strømme, M. Effects of amine modification of mesoporous magnesium carbonate on controlled drug release. *Int J Pharm*. **2017**, 524(1-2):141-7. https://doi.org/0.1016/j.ijpharm.2017.03.063

[29] Vall, M., Ferraz, N., Cheung, O., Strømme, M., Zardán Gómez de la Torre, T. Exploring the use of amine modified mesoporous magnesium carbonate for the delivery of salicylic acid in topical formulations: in vitro cytotoxicity and drug release studies. *Molecules*. **2019**, 24(9):1820. https://doi.org/10.3390/molecules24091820

[30] Vall, M., Strømme, M., Cheung, O. Amine-modified mesoporous magnesium carbonate as an effective adsorbent for Azo dyes. *ACS Omega*. **2019**, 4(2):2973-9. https://doi.org/10.1021/acsomega.8b03493

[31] Thommes, M., Kaneko, K., Neimark, A. V., Olivier, J. P., Rodriguez-Reinoso, F., Rouquerol, J., Sing, K. S. W. Physisorption of gases, with special reference to the evaluation of surface area and pore size distribution (IUPAC Technical Report). *Pure Appl Chem*. **2015**, 87(9-10):1051-69. https://doi.org/10.1515/pac-2014-1117

[32] Wang, J., Xia, Y. Fe-Substituted Isoreticular Metal–Organic Framework for Efficient and Rapid Removal of Phosphate. *ACS Appl Nano Mater*. **2019**, 2(10):6492-502. https://doi.org/10.1021/acsanm.9b01429

[33] Nehra, M., Dilbaghi, N., Singhal, N. K., Hassan, A. A., Kim, K. H., Kumar, S. Metal organic frameworks MIL-100(Fe) as an efficient adsorptive material for phosphate management. *Environ Res*. **2019**, 169:229-36. https://doi.org/10.1016/j.envres.2018.11.013

[34] Li, J., Chang, H., Li, Y., Li, Q., Shen, K., Yi, H., Zhang, J. Synthesis and adsorption performance of La@ZIF-8 composite metal–organic frameworks. *RSC Adv*. **2020**, 10(6):3380-90. https://doi.org/10.1039/c9ra10548d

[35] Yang, Q., Wang, X., Luo, W., Sun, J., Xu, Q., Chen, F., Zhao, J., Wang, S., Yao, F., Wang, D., Li, X., Zeng, G. Effectiveness and mechanisms of phosphate adsorption on iron-modified biochars derived from waste activated sludge. *Bioresour Technol*. **2018**, 247:537-44. https://doi.org/10.1016/j.biortech.2017.09.136

[36] Zhang, G., Liu, H., Liu, R., Qu, J. Removal of phosphate from water by a Fe-Mn binary oxide adsorbent. *J Colloid Interface Sci*. **2009**, 335(2):168-74. https://doi.org/10.1016/j.jcis.2009.03.019

[37] Almasri, D. A., Saleh, N. B., Atieh, M. A., McKay, G., Ahzi, S. Adsorption of phosphate on iron oxide doped halloysite nanotubes. *Sci Rep*. **2019**, 9(1):3232. https://doi.org/10.1038/s41598-019-39035-2

[38] Koh, K. Y., Zhang, S., Paul Chen, J. Hydrothermally synthesized lanthanum carbonate nanorod for adsorption of phosphorus: Material synthesis and optimization, and demonstration of excellent performance. *Chem Eng J*. **2020**, 380. https://doi.org/10.1016/j.cej.2019.122153

[39] Xu, R., Zhang, M., Mortimer, R. J., Pan, G. Enhanced Phosphorus Locking by Novel Lanthanum/Aluminum-Hydroxide Composite: Implications for Eutrophication Control. *Environ Sci Technol*. **2017**, 51(6):3418-25. https://doi.org/10.1021/acs.est.6b05623

[40] Haghseresht, F., Wang, S., Do, D. D. A novel lanthanum-modified bentonite, Phoslock, for phosphate removal from wastewaters. *Appl Clay Sci*. **2009**, 46(4):369-75. https://doi.org/10.1016/j.clay.2009.09.009

[41] Karaca, S., Gurses, A., Ejder, M., Acikyildiz, M. Adsorptive removal of phosphate from aqueous solutions using raw and calcinated dolomite. *J Hazard Mater*. **2006**, 128(2-3):273-9. https://doi.org/10.1016/j.jhazmat.2005.08.003

[42] Delaney, P., McManamon, C., Hanrahan, J. P., Copley, M. P., Holmes, J. D., Morris, M. A. Development of chemically engineered porous metal oxides for phosphate removal. *J Hazard Mater*. **2011**, 185(1):382-91. https://doi.org/10.1016/j.jhazmat.2010.08.128

[43] Xu, N., Li, Y., Zheng, L., Gao, Y., Yin, H., Zhao, J., Chen, Z., Chen, J., Chen, M. Synthesis and application of magnesium amorphous calcium carbonate for removal of high concentration of phosphate. *Chem Eng J*. **2014**, 251:102-10. https://doi.org/10.1016/j.cej.2014.04.037

Supporting information

Amorphous mesoporous calcium carbonate and magnesium carbonate as effective sorbents for the removal of phosphate in aqueous solutions

Eveline Croket, Michelle Åhlén, Maria Strømme, Ocean Cheung*

Division of Nanotechnology and Functional Materials, Department of Materials Science and Engineering, Ångström Laboratory, Uppsala University SE-751 03, Sweden.

*Corresponding author. Tel.: +46 18 471 3279, E-mail: ocean.cheung@angstrom.uu.se

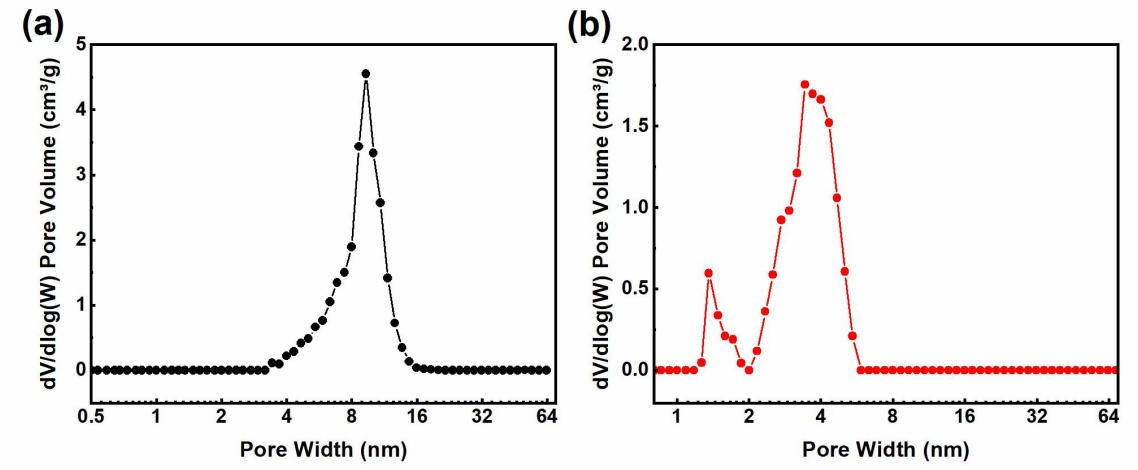

Figure S1. Pore size distributions of (a) HPACC and (b) MMC.

Table S1. Pore volume of HPACC and MMC.

Material	Total pore volume (cm³/g)
HPACC	0.868
MMC	0.482